Mathematical Medicine and Biology (2009) **26**, 165–185
doi:10.1093/imammb/dqp008
Advance Access publication on April 7, 2009

A mathematical model for the deformation of the eyeball by an elastic band

STEPHEN L. KEELING† AND GEORG PROPST‡
Institut für Mathematik und Wissenschaftliches Rechnen, Karl-Franzens-Universität Graz, Heinrichstraße 36, 8010 Graz, Austria

GEORG STADLER§
Institute for Computational Engineering and Sciences, University of Texas at Austin, 1 University Station, C0200 Austin, TX 78712, USA

AND

WERNER WACKERNAGEL¶
Universitäts-Augenklinik, Medizinische Universität Graz, Auenbruggerplatz 4, 8036 Graz, Austria

[Received on 30 May 2008; revised on 16 December 2008; accepted on 3 March 2009]

In a certain kind of eye surgery, the human eyeball is deformed sustainably by the application of an elastic band. This article presents a mathematical model for the mechanics of the combined eye/band structure along with an algorithm to compute the model solutions. These predict the immediate and the lasting indentation of the eyeball. The model is derived from basic physical principles by minimizing a potential energy subject to a volume constraint. Assuming spherical symmetry, this leads to a two-point boundary-value problem for a non-linear second-order ordinary differential equation that describes the minimizing static equilibrium. By comparison with laboratory data, a preliminary validation of the model is given.

Keywords: mathematical model; eyeball; cerclage.

1. Introduction

In this article, the deformation of the human eyeball that is caused by the application of an elastic band is considered. The vertical circumferential application of a closed elastic band, called a cerclage, around the eyeball is a common clinical practice. Its purpose is to dent the eyeball such that an existing retinal separation is reduced or reversed.

In rhegmatogenous retinal detachment, the neurosensory retina loses contact to the underlying retinal pigment epithelium, with fluid from the liquefied vitreous entering and expanding the potential space between those membranes through a break in the retina. The pathomechanism of retinal detachment was discovered by Gonin (1920) at the beginning of the 20th century. Gonin also realized that sealing the retinal break is essential for successful reattachment of the retina. Over the following years and decades, a number of methods for closing retinal breaks were developed. Scleral buckling procedures gained

†Email: stephen.keeling@uni-graz.at
‡Corresponding author. Email: georg.propst@uni-graz.at
§Email: georgst@ices.utexas.edu
¶Email: werner.wackernagel@meduni-graz.at

widespread acceptance and in the 1940s, Schepens introduced the use of encircling bands (cerclage) for a 360° buckling of the sclera (Schepens *et al.*, 1957). Currently, scleral buckling procedures are being compared against newer surgical techniques in a large multicentre clinical trial (Heimann *et al.*, 2007). To interpret clinical outcome, it is essential to understand the mechanical effects of buckling surgery. The mathematical model we present for the effects of an encircling elastic band can provide some deeper insight into the mechanics of retinal detachment surgery. At the beginning of the procedure, the conjunctiva is opened along the corneal limbus. The sclera is easily accessible, as the eyeball is not encased by a tight membrane, but is loosely embedded in the intraorbital fat, surrounded by thin fibrous sheaths providing sufficient space for effortless eye movements. This episcleral space (Tenon's space) between the sclera and the episcleral sheets is opened next during surgery. Then, the four straight eye muscles are exposed and the elastic band is sutured to the outside of the sclera beneath the muscles. Care must be taken that the sutures keep the band in place, but do not hinder longitudinal movements of the band, as the next step is to tighten the band. This means pulling the overlapping ends of the elastic band into opposite directions, thus shortening the band, and then securing the band in this tightened state with a locking suture.

The immediate effect of the application of the stretched narrow band is a slight indentation of the sclera and the choroid beneath the band and an increase of the intraocular pressure. After the surgery, in the course of a day, the intraocular pressure goes back to its nominal value by autoregulated decrease of aqueous humour and vitreous within the eyeball. When the pressure eventually is back to the nominal value, the indentation of the sclera by the band is deeper than immediately after surgery. It is left to the expertise of the surgeon to predict the final deformation of the eyeball as well as the magnitude of the intraocular pressure immediately caused by the application of the stretched band. In many instances, a deep final indentation is desirable, but the intraocular pressure at surgery must be kept within a physiologically admissible range.

The purpose of the present article is to establish a mathematically formulated model for the deformation of the eyeball that allows us to model the mechanisms during and after the surgery described above. In order to set the stage for our approach, we begin by briefly describing another approach which is extremely simple and yet another which is relatively complex. First, a simple model is obtained as follows. If all forces due to the deformation of the sclera and the choroid were neglected, the intraocular pressure and the band forces would be at equilibrium. Thus, a simple estimate of the intraocular pressure at surgery is the force per unit area that is exerted by the cerclage. Furthermore, the indentation when the pressure is back to its nominal value could be estimated by determining the radius of the stretched annular band when its exerted force is equal to the nominal pressure. Both these estimates can be done by back-of-the-envelope calculations using the material parameters of the band. However, these estimates are far off the physical data that are described in Section 5.2. Therefore, the forces due to the ocular rigidity and the deformation of the membrane have to be taken into account. On the other hand, a relatively complex model is obtained by representing the sclera and choroid with finite thicknesses, modelling these with finite elements and carrying out a detailed force balance or energy minimization (Alastrué *et al.*, 2006; Pandolfi & Manganiello, 2006; Seo *et al.*, 2003). Intermediate between the levels of complexity of these alternative approaches, our model treats the surface of the eyeball as a membrane of negligible thickness in which non-linear elastic effects are incorporated.

While still being relatively simple, this formulation requires and enhances the understanding of the detailed mechanics of the system under investigation. Furthermore, our simulation tool facilitates an enhanced intuitive conception of the eyeball–band configuration for clinicians. In order to validate our mathematical model, its predictions are compared to physical data, acquired in laboratory measurements

on enucleated human eyes. The quantitative congruence of the predictions and the data indicates that the model could be used to predict the short- and long-term effect of the elastic band. Ideally, the model and the simulation tool will provide the surgeon with a patient-specific prediction of the final (i.e. postoperative) indentation. This facilitates the choice of the appropriate material properties of the cerclage and helps the surgeon to decide on the initial stretch.

To the best of our knowledge, no mathematical model that combines the eyeball and an elastic band is found in the literature. However, much information is available on the anatomy, physiology and mechanics of the human eye (see, e.g. Bryant & McDonnell, 1996; Elsheikh *et al.*, 2008a,b; Hoeltzel *et al.*, 1992). In addition to this information, we rely on the classical theory of surface phenomena (Pellicer *et al.*, 1995). In fact, we model the eyeball as a spherical elastic membrane. This is an idealized approximation because a real eyeball is not strictly spherical nor strictly rotationally symmetric. Moreover, the thickness of the eye's covering is not constant as in our model, but varies between 0.3 and 1.3 mm (e.g. Collins & van der Werff, 1980, p. 2) and we neglect the anisotropy of the cornea and sclera (Elsheikh *et al.*, 2008b; Pinsky *et al.*, 2005). Our idealized approximations are motivated by the simplicity of the resulting model and the relative ease of its analytic and numerical use, and it is, to some extent, justified by the agreement of our model's predictions with physical measurements. The amount by which the predictions differ, when working with a geometrically and physically more realistic, higher dimensional model, may be demonstrated by implementing such a model, but this is not the subject of the present article.

In our model, the sphere contains a given volume of incompressible fluid and is deformed by the forces of the elastic band. The physically appropriate deformation is one which minimizes potential energy under a constant-volume constraint. The optimality system for the associated Lagrangian function is a non-linear 1D second-order ordinary differential equation with an integral constraint. This optimality system is discretized by finite differences and is solved using an approximate Newton iteration. This solution process provides a mapping from the 'preoperative' state to the 'intraoperative' state which develops immediately after the cerclage operation. To invert this mapping in order to find the volume of a spherical band-free eyeball corresponding to a specified band-loaded state, we use a simple bisection iteration. We use this bisection approach to find a reduced volume resulting from autoregulation and corresponding to a band-loaded 'postoperative' state with a normal pressure. The associated geometry is our prediction of the membrane shape and indentation in the postoperative state. By comparison with laboratory data, a preliminary validation of the model is given.

2. The model

To address the clinical questions posed in Section 1, a mathematical model is developed here which addresses the following three phases of the cerclage operation, which are diagrammed in Fig. 1.

- Preoperative phase: The eyeball is spherical with a fixed radius r_1 and thus a fixed volume V_1 of incompressible fluid. The outer surface of the eyeball is elastic, and the eye has a normal inner pressure p_1.
- Intraoperative phase: Immediately after the cerclage has been fastened tautly to the eyeball, the band applies a certain force to the eye. Because of the elasticity of the outer surface of the eye, the band force creates a deformation in the surface geometry including an indentation around the band. Adding to the force of the existing tension in the outer surface, the band force increases the internal pressure from p_1 to $p > p_1$, which must not be so high as to cause damage to the eye. Since the fluid inside the eyeball is incompressible, the volume V_1 remains unchanged.

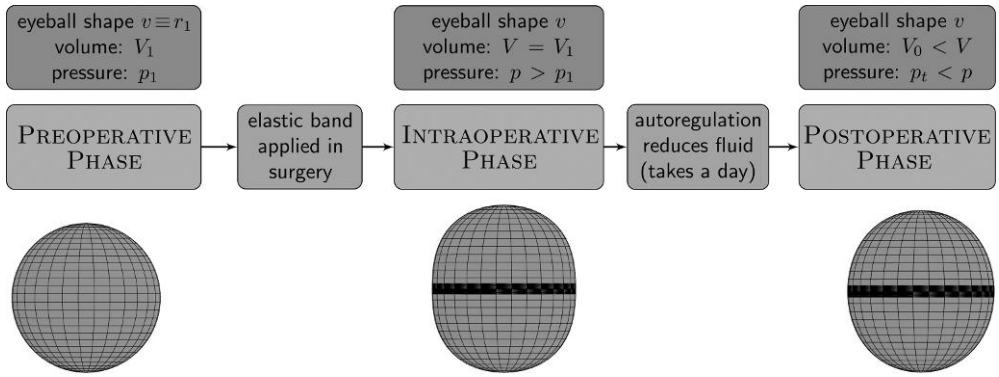

FIG. 1. Schematic sequence of the three stationary states before, during and after applying the cerclage to the eyeball.

- Postoperative phase: Within a day, an autoregulation mechanism reduces the volume of fluid in the eye from V_1 to $V_0 < V_1$ and thereby brings the pressure from p down to a target pressure $p_t < p$, typically equal to the normal pressure $p_t = p_1$. At this point, the indentation of the eyeball surface around the band is deeper than intraoperatively. Also, if the band was removed and the surface was returned to spherical shape, the radius would be r_0 corresponding to the volume V_0 and the pressure would be $p_0 < p_t$.

As indicated with respect to the preoperative phase, the undistorted eyeball is approximated here by a perfect sphere. Its surface is modelled to be a physically homogeneous elastic membrane of small thickness. The interior of the membrane is filled with homogeneous incompressible fluid. All other anatomic features are neglected. In view of the model's purpose and on the basis of related material found in Blyth & Pozrikidis (2004), Bryant & McDonnell (1996), Collins & van der Werff (1980), Elsheikh *et al.* (2008a), Friberg & Lace (1988), Purslow & Karwatowski (1996) and Schmitz-Valckenberg & Meyer-Schwickerath (1975), we believe that these simplifications lead to a model which is still sufficiently close to reality. The assumptions on the cerclage are that it is a linearly elastic band of rectangular cross-section. For the range of strains and time scales that are considered here, the validity of this assumption was confirmed in systematic physical measurements of elasticity by Messphysik Materials Testing GmbH (Altenmarkt bei Fürstenfeld, Austria). The encircling bands were provided by FCI Ophthalmics. We do not model any friction between the sphere and the band as frictionless fixation of the band to the sclera is one goal of the surgical procedure and can be observed and checked during surgery when the elastic band is tightened.

For the mathematical description of the system, a spherical coordinate system (r, θ, ϕ) is used with origin in the centre of the undistorted sphere as illustrated in Fig. 2. The rectangular (x, y, z) and cylindrical coordinates (R, θ, z) are also used when convenient, where the vertical axis in Fig. 2 is the z-axis, which is perpendicular to the (x, y)-plane coinciding with the polar (R, θ)-plane. The ray $\phi = 0$ crosses the membrane where the eyeball would have its pupil, and the circular band is located perpendicular to this ray within $z_1 \leqslant z \leqslant z_2$. Typically, the configuration is equatorial, i.e. $z_1 = -z_2$, and the band is narrow. When the band is attached to the sphere, the coupled system is in equilibrium if and only if the forces due to the deformation of the sphere and the forces due to the strain of the band cancel each other.

Let r_1 be the radius of the undistorted sphere and $\hat{R}$ be the rest radius of the cylindrical band when no forces are applied. Both are given parameters. The sphere stretches the band if $r_1 > \hat{R}$. Let $v(\theta, \phi)$

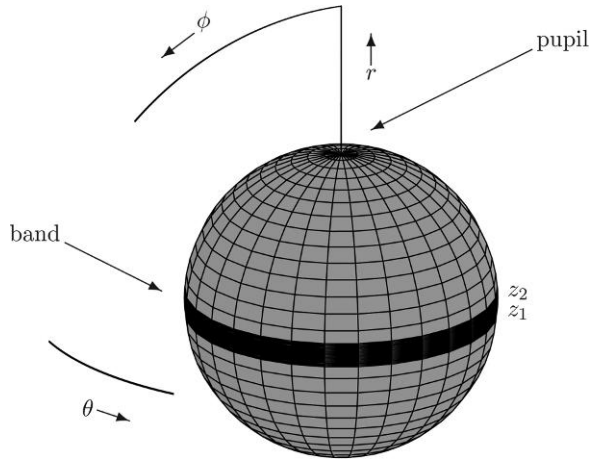

FIG. 2. Spherical coordinates (r, θ, ϕ) are used to represent the model geometry. The pupil is centred at $\phi = 0$ and the cerclage lies on the surface between $\phi_1 \leqslant \phi \leqslant \phi_2$. All model variables are assumed to be independent of θ.

denote the r-coordinate of the distorted membrane at the location (θ, ϕ). Because the configuration is rotationally symmetric with respect to the z-axis, υ will not depend on θ. Thus, $\upsilon = \upsilon(\phi)$.

The force per unit area exerted by the band when it is stretched to radius $R \geqslant \hat{R}$ is given as follows. Under the assumption that the band remains cylindrical, let $\hat{L}_\mathrm{b} = 2\pi\hat{R}$ be the rest length of the band while $L_\mathrm{b} = 2\pi R$ is the stretched length. The band has a width $\omega_\mathrm{b} = z_2 - z_1$ and a small thickness δ_b, so the area of the cross-section of the band is $A_\mathrm{b} = \omega_\mathrm{b}\delta_\mathrm{b}$. Using the Young's modulus E_b of the band, the tangential force in the stretched band is given by $F_\mathrm{tan} = E_\mathrm{b}A_\mathrm{b}(L_\mathrm{b} - \hat{L}_\mathrm{b})/\hat{L}_\mathrm{b} = E_\mathrm{b}\omega_\mathrm{b}\delta_\mathrm{b}(R - \hat{R})/\hat{R}$. Then, the force per unit width, or tension, through a rectangular cross-section in the stretched band is $F_\mathrm{tan}/\omega_\mathrm{b} = E_\mathrm{b}\delta_\mathrm{b}(L_\mathrm{b} - \hat{L}_\mathrm{b})/\hat{L}_\mathrm{b}$. According to the Laplace law for a cylinder (Adamson, 1997), this tension is related to the force per unit area f directed towards the central axis of the cylindrical band according to $F_\mathrm{tan}/\omega_\mathrm{b} = Rf$ or $f = E_\mathrm{b}\delta_\mathrm{b}(R - \hat{R})/(R\hat{R})$. Thus, the vectorial force of the band is given by

$$\boldsymbol{f} = -\boldsymbol{e}_R\, f(\upsilon \sin\phi, z), \qquad f(R, z) = \begin{cases} E_\mathrm{b}\delta_\mathrm{b}\left(\frac{1}{\hat{R}} - \frac{1}{R}\right), & z_1 \leqslant z \leqslant z_2, \\ 0, & \text{otherwise}, \end{cases} \tag{2.1}$$

where

$$\boldsymbol{e}_R = \langle \cos\theta, \sin\theta, 0 \rangle^\top \tag{2.2}$$

are the rectangular components of the unit vector directed from the z-axis towards the cylindrical band. Note that the bending stiffness of the band or its resistance to a departure from cylindrical shape is not explicitly modelled here. Thus, the band may depart mildly from a strictly cylindrical shape, and thus, (2.1) is obtained by repeating the above argument for infinitesimally small cylindrical sections of the band.

For the undistorted sphere with volume $V_1 = 4\pi r_1^3/3$ and radius $\upsilon \equiv r_1$, the relation between the internal pressure p_1 and the tension T_1 in the elastic membrane is given by Laplace's law for the sphere (Adamson, 1997),

$$2T_1 = p_1 r_1. \tag{2.3}$$

When the volume of the internal incompressible fluid is varied, the variation of the intraocular pressure can be modelled by $\ln(p/p_1) = \sigma(V - V_1)$, where σ is called Friedenwald's coefficient of ocular rigidity (Collins & van der Werff, 1980). Since Friedenwald's formula is used in the present context only for the band-free spherical eyeball, the formula is written in the following form for spherical volumes:

$$\ln \frac{p}{p_1} = \frac{4\pi\sigma}{3}(r^3 - r_1^3), \tag{2.4}$$

where p is the pressure in the spherical eyeball with radius r.

When the membrane is no longer spherical, the local tension is determined by the following proposed perturbation of (2.3):

$$T(\upsilon) = T_0 + E_{\mathrm{m}}\delta_{\mathrm{m}}\left[\frac{S(\upsilon)}{S(r_0)} - 1\right], \quad T_0 = T_0(\upsilon), \;\; r_0 = r_0(\upsilon). \tag{2.5}$$

Here, $r_0(\upsilon)$ is determined from the constant-volume condition seen below in (2.25),

$$r_0^3 = \frac{1}{2}\int_0^{\pi} \upsilon^3 \sin\phi \, \mathrm{d}\phi, \tag{2.6}$$

while $T_0(\upsilon)$ is determined from r_0 using (2.4) and (2.3),

$$T_0 = \frac{1}{2} r_0 p_0 = \frac{1}{2} r_0 p_1 \exp\left[\frac{4\pi\sigma}{3}(r_0^3 - r_1^3)\right]. \tag{2.7}$$

Then, $S(\upsilon)$ denotes the surface area of the eyeball with geometry υ:

$$S(\upsilon) = \int_0^{2\pi}\int_0^{\pi} \upsilon \sin\phi \sqrt{\upsilon^2 + \upsilon_\phi^2}\, \mathrm{d}\phi \, \mathrm{d}\theta = 2\pi \int_0^{\pi} \upsilon \sin\phi \sqrt{\upsilon^2 + \upsilon_\phi^2}\, \mathrm{d}\phi, \tag{2.8}$$

where the surface element in the first integral is given below in (2.12). In (2.5), E_{m} is the Young's modulus and δ_{m} is the thickness of the scleral membrane. Note that the system of equations (2.5–2.8) establishes a non-linear relation between the geometry υ and the proposed spatially invariant tension $T(\upsilon)$. The relation (2.5) is postulated on the basis of dimensional analysis as follows. Specifically, a relative expansion is required next to $E_{\mathrm{m}}\delta_{\mathrm{m}}$, and any relative expansion other than with respect to surface area can be ruled out with the assumptions that the tension is spatially invariant and increases when the surface area is increased. For instance, a relative volume expansion is not appropriate in place of $[S(\upsilon)/S(r_0(\upsilon)) - 1]$ since such a formula would leave the tension unchanged at constant volume and varying surface area. Also, if certain lengths were defined in the membrane and a relative length expansion were used in place of $[S(\upsilon)/S(r_0(\upsilon)) - 1]$, this could lead to a spatially varying tension. The tension still satisfies the usual relation to mean curvature seen below in (2.26), but a constitutive relation, given by (2.5–2.8), is required to determine the tension and geometry simultaneously.

In what follows, we derive a model for the geometry of the membrane by minimizing the mechanical potential energy (Pellicer *et al.*, 1995) under the constraint of a given internal volume. A slightly different formulation, which is also based on a minimal energy formulation (without a volume constraint), is discussed in Blyth & Pozrikidis (2004). Note that force balancing methods (as used, e.g. in Preston *et al.*, 2008) represent an interesting alternative to energy minimization methods. However, the integration of constraints in these methods is usually more difficult.

To derive our model, we suppose that a small membrane element $\mathcal{S}$ is disturbed from equilibrium by a change $\mathrm{d}\mathcal{S}$ in surface area and a change $\mathrm{d}\mathcal{V}$ in volume of the eyeball. These perturbations $\mathrm{d}\mathcal{V}$ and $\mathrm{d}\mathcal{S}$ from the equilibrium state increase the potential energy $\mathcal{F}$ of the band-eyeball-system as follows,

$$d\mathcal{F} = T\,\mathrm{d}\mathcal{S} - F\,\mathrm{d}\mathcal{V} \tag{2.9}$$

and this increased potential energy is then available for work to return the system to equilibrium. Specifically, $-F\,\mathrm{d}\mathcal{V}$ is the work performed by the force per unit area $-F$ external to the membrane (i.e. band plus pressure forces) to return the membrane element to its equilibrium state once its volume is perturbed by $\mathrm{d}\mathcal{V}$. Also, $T\,\mathrm{d}\mathcal{S}$ is the work performed by the membrane tension or force per unit length T to return the membrane element to its equilibrium state once its area is perturbed by $\mathrm{d}\mathcal{S}$.

For the band-loaded equilibrium state, let v denote the radial function representing the eyeball geometry, and let p denote the corresponding intraocular pressure. Then, according to (2.9), the mechanical potential energy $\mathcal{F}$ of the band–eyeball system has a variational derivative with respect to v for a perturbation $\bar{v}$ in the membrane element $\mathcal{S}$ which is given by

$$\frac{\delta\mathcal{F}}{\delta v}(v;\bar{v}) = T(v)\frac{\delta\mathcal{S}}{\delta v}(v;\bar{v}) - F(v,p)\frac{\delta\mathcal{V}}{\delta v}(v;\bar{v}). \tag{2.10}$$

These components of the potential energy of the band–eyeball system are determined explicitly as follows.

To obtain the geometrical constructions required below, recall that the radial coordinate $v(\phi)$ of the eye is assumed to be independent of θ. Then, note that when the membrane surface is expressed in terms of the Cartesian coordinate vector according to

$$\boldsymbol{X}(\phi,\theta;v) = \langle v(\phi)\cos\theta\sin\phi,\, v(\phi)\sin\theta\sin\phi,\, v(\phi)\cos\phi\rangle^{\top}, \tag{2.11}$$

the surface element is given by

$$\begin{aligned}\mathcal{S}(v) &= |\boldsymbol{X}_{\phi}(\phi,\theta;v)\times\boldsymbol{X}_{\theta}(\phi,\theta;v)|\,\mathrm{d}\phi\,\mathrm{d}\theta\\ &= v\sin\phi\sqrt{v^2+v_{\phi}^2}\,\mathrm{d}\phi\,\mathrm{d}\theta\end{aligned} \qquad \text{or} \quad \frac{\delta\mathcal{S}}{\delta v}(v;\bar{v}) = \frac{2v^2\bar{v}+\bar{v}v_{\phi}^2+vv_{\phi}\bar{v}_{\phi}}{\sqrt{v^2+v_{\phi}^2}}\sin\phi\,\mathrm{d}\phi\,\mathrm{d}\theta \tag{2.12}$$

and the outwardly directed unit vector normal to the membrane at (v,θ,ϕ) is given by

$$\begin{aligned}\boldsymbol{n}(v) &= \frac{\boldsymbol{X}_{\phi}(\phi,\theta;v)\times\boldsymbol{X}_{\theta}(\phi,\theta;v)}{|\boldsymbol{X}_{\phi}(\phi,\theta;v)\times\boldsymbol{X}_{\theta}(\phi,\theta;v)|}\\ &= \frac{1}{\sqrt{v^2+v_{\phi}^2}}\langle -\cos\theta(v\cos\phi)_{\phi}, -\sin\theta(v\cos\phi)_{\phi}, (v\sin\phi)_{\phi}\,\rangle^{\top}.\end{aligned} \tag{2.13}$$

Also, the volume element in the cone from the origin to $\mathcal{S}(v)$ is given by

$$\mathcal{V}(v) = \sin\phi\,\mathrm{d}\phi\,\mathrm{d}\theta\int_0^{v(\phi)} r^2\,\mathrm{d}r \quad \text{or} \quad \frac{\delta\mathcal{V}}{\delta v}(v;\bar{v}) = \bar{v}v^2\sin\phi\,\mathrm{d}\phi\,\mathrm{d}\theta. \tag{2.14}$$

Equipped with these geometric components, consider first $-F(v,p)\delta\mathcal{V}/\delta v(v;\bar{v})$. When the membrane is positioned at $v(\phi)$ with the pressure p, the sum of outwardly directed normal forces per unit area, external to the membrane, is $F(v,p) = p - f(v\sin\phi, v\cos\phi)\boldsymbol{e}_R^{\top}\boldsymbol{n}(v)$, where

$$-f(v\sin\phi, v\cos\phi)\boldsymbol{e}_R^{\top}\boldsymbol{n}(v) = f(v\sin\phi, v\cos\phi)\frac{(v\cos\phi)_{\phi}}{\sqrt{v^2+v_{\phi}^2}} \tag{2.15}$$

is the membrane normal component of the band force. The variation $\delta\mathcal{V}/\delta v(v;\bar{v})$ is given by (2.14). By summing $-F(v,p)\delta\mathcal{V}/\delta u(v;\bar{v})$ over all membrane elements $\mathcal{S}$, the variational derivative of the potential energy in the presence of forces external to the membrane is given by

$$\frac{\delta V_{\mathrm{e}}}{\delta v}(v;\bar{v}) = -2\pi \int_0^\pi \left\{ f(v\sin\phi, v\cos\phi)\frac{(v\cos\phi)_\phi}{\sqrt{v^2+v_\phi^2}} + p \right\} \bar{v} v^2 \sin\phi \,\mathrm{d}\phi. \tag{2.16}$$

Now, consider $T(v)\delta\mathcal{S}/\delta v(v;\bar{v})$. When the membrane is positioned at $v(\phi)$, the membrane tension $T(v)$ is given by (2.5). The variation $\delta\mathcal{S}/\delta v(v;\bar{v})$ is given by (2.12). By summing $T(v)\delta\mathcal{S}/\delta v(v;\bar{v})$ over all membrane elements $\mathcal{S}$, the variational derivative of the potential energy in the presence of forces internal to the membrane is given by

$$\frac{\delta V_{\mathrm{i}}}{\delta v}(v;\bar{v}) = 2\pi \int_0^\pi T(v) \left\{ \frac{2v^2\bar{v} + \bar{v}v_\phi^2 + vv_\phi\bar{v}_\phi}{\sqrt{v^2+v_\phi^2}} \right\} \sin\phi \,\mathrm{d}\phi. \tag{2.17}$$

Now, consider the incompressibility constraint. For a given radius r_1 of the undistorted sphere, the constant-volume condition requires that

$$V_{\mathrm{c}}(v) = \int_0^{2\pi}\int_0^\pi \int_0^{v(\phi)} r^2 \sin\phi \,\mathrm{d}r \,\mathrm{d}\phi \,\mathrm{d}\theta - \frac{4\pi r_1^3}{3} = \frac{2\pi}{3}\int_0^\pi v^3 \sin\phi \,\mathrm{d}\phi - \frac{4\pi r_1^3}{3} = 0. \tag{2.18}$$

To minimize the potential energy $V_{\mathrm{e}}(u) + V_{\mathrm{i}}(u)$ subject to $V_{\mathrm{c}}(u) = 0$, the following Lagrangian function

$$L(v,\lambda) = \frac{1}{2\pi}[V_{\mathrm{e}}(v) + V_{\mathrm{i}}(v) - \lambda V_{\mathrm{c}}(v)] \tag{2.19}$$

is required to be stationary in v

$$\begin{aligned} 0 = \frac{\delta L}{\delta v}(v;\bar{v}) = \int_0^\pi T(v) \left\{ \frac{2v^2\bar{v} + \bar{v}v_\phi^2 + vv_\phi\bar{v}_\phi}{\sqrt{v^2+v_\phi^2}} \right\} \sin\phi \,\mathrm{d}\phi \\ - \int_0^\pi \bar{v} \left\{ f(v\sin\phi, v\cos\phi)\frac{(v\cos\phi)_\phi}{\sqrt{v^2+v_\phi^2}} + (p_1+\lambda) \right\} v^2 \sin\phi \,\mathrm{d}\phi, \quad \forall \bar{v} \in \mathcal{H}^1([0,\pi]), \end{aligned} \tag{2.20}$$

and in the Lagrange multiplier λ

$$0 = \frac{\delta L}{\delta \lambda}(\lambda;\bar{\lambda}) = -\frac{\bar{\lambda}}{3}\int_0^\pi v^3 \sin\phi \,\mathrm{d}\phi + \frac{2\bar{\lambda}r_1^3}{3}, \quad \forall \bar{\lambda} \in \boldsymbol{R}, \tag{2.21}$$

where $\bar{v}$ and $\bar{\lambda}$ are perturbations of v and λ and p_1 is used in (2.20) consistent with the r_1 in (2.21) and (2.4). The space $\mathcal{H}^1([0,\pi])$ in (2.20) is defined as follows. In order to formulate the optimality system more precisely, membrane geometries are considered to lie in a Sobolev space $H^\nu(S^2)$ of functions whose weak derivatives up to order ν are Lebesgue square integrable on the sphere S^2, i.e. in

$L^2(S^2)$. Because of the θ-independence of membrane geometries, these Sobolev spaces can be reduced to weighted Sobolev spaces $\mathcal{H}^\nu([0,\pi])$ on the interval $[0,\pi]$ equipped with the inner product

$$(u,v)^2_{\mathcal{H}^\nu([0,\pi])} = \sum_{m=0}^{\nu} \int_0^\pi D_\phi^m u D_\phi^m v \sin\phi \, \mathrm{d}\phi, \tag{2.22}$$

where D_ϕ^m denotes the mth derivative with respect to ϕ. In particular, under conditions given explicitly in Appendix A, the right side of (2.20) is well defined for $\bar{v}$, $v \in \mathcal{H}^1([0,\pi])$. Also, provided $v \in \mathcal{H}^2([0,\pi])$, the optimality condition (2.20) can be expressed as a pointwise differential condition on v by integrating (2.20) by parts as follows:

$$\frac{\delta L}{\delta v}(v;\bar{v}) = \int_0^\pi \bar{v} \left\{ T(v) \left[\frac{2v^2 + v_\phi^2}{\sqrt{v^2+v_\phi^2}} \right] - \left[f(v\sin\phi, v\cos\phi) \frac{(v\cos\phi)_\phi}{\sqrt{v^2+v_\phi^2}} + (p_1+\lambda) \right] v^2 \right\} \sin\phi \, \mathrm{d}\phi$$
$$- \int_0^\pi \bar{v} \left\{ T(v)\sin\phi \frac{v v_\phi}{\sqrt{v^2+v_\phi^2}} \right\}_\phi \mathrm{d}\phi + \bar{v} \left\{ T(v)\sin\phi \frac{v v_\phi}{\sqrt{v^2+v_\phi^2}} \right\} \Bigg|_{\phi=0}^{\phi=\pi}. \tag{2.23}$$

When $v \in \mathcal{H}^2([0,\pi])$ holds, then (2.20) and (2.23) imply that

$$- \left\{ T(v) \frac{v v_\phi}{\sqrt{v^2+v_\phi^2}} \sin\phi \right\}_\phi + T(v) \frac{2v^2+v_\phi^2}{\sqrt{v^2+v_\phi^2}} \sin\phi$$
$$= \left\{ f(v\sin\phi, v\cos\phi) \frac{(v\cos\phi)_\phi}{\sqrt{v^2+v_\phi^2}} + (p_1+\lambda) \right\} v^2 \sin\phi, \quad 0 < \phi < \pi,$$
$$v_\phi = 0, \quad \phi = 0, \pi. \tag{2.24}$$

In particular, the boundary condition is derived by choosing $\bar{v}$ in (2.23) to vanish in most of the interval $(0,\pi)$ while satisfying $\bar{v}\sin\phi \approx 1$ on the boundary. The optimality condition that (2.21) holds for all $\bar{\lambda} \in \boldsymbol{R}$ implies the condition

$$\int_0^\pi v^3 \sin\phi \, \mathrm{d}\phi = 2r_1^3. \tag{2.25}$$

Now, suppose that $v \in \mathcal{H}^2([0,\pi])$ and $p \in \boldsymbol{R}$ satisfy (2.25) and

$$- \left\{ \frac{T(v) v v_\phi \sin\phi}{\sqrt{v^2+v_\phi^2}} \right\}_\phi + \frac{T(v)v^2\sin\phi}{\sqrt{v^2+v_\phi^2}} + T(v)\sin\phi\sqrt{v^2+v_\phi^2}$$
$$= \left[f(v\sin\phi, v\cos\phi) \frac{(v\cos\phi)_\phi}{\sqrt{v^2+v_\phi^2}} + p \right] v^2 \sin\phi, \quad 0 < \phi < \pi, \ v_\phi = 0, \ \phi = 0, \pi. \tag{2.26}$$

Then, the radial function v and the constant internal pressure $p = p_1 + \lambda$ satisfy (2.25) and (2.24) with $\lambda = 0$, and the Lagrangian function is stationary in $(v, 0)$. Since $\lambda = 0$ holds, the constraint (2.25) is not active but rather it is fulfilled naturally by the geometry and the pressure satisfying (2.25) and (2.26). Therefore, the mathematical problem to be solved for the intraoperative state is to seek a radial function v and a constant internal pressure p which satisfy (2.25) and (2.26).

Thus, after computing v and p from (2.25) and (2.26) for a given r_1 in (2.25), define the cerclage operator

$$\mathcal{C}(r_1) = (v, p) \tag{2.27}$$

which to a given band-free eyeball radius r_1 in (2.25) assigns the new geometry $\mathcal{C}(r_1)[v]$ and the new pressure $\mathcal{C}(r_1)[p]$ after the band is applied. Since a band-free eyeball radius r_1 and pressure p_1 are related by (2.4), it follows that the mapping from p_1 to the solution (v, p) to (2.25) and (2.26) is also given by $\mathcal{C}(r_1)$.

For the postoperative state, it is assumed that the volume of the eyeball is reduced by physiological autoregulation to V_0 at which the pressure is reduced from $\mathcal{C}(r_1)[p]$ to a target pressure p_t, which is typically equal to the original pressure $p_t = p_1$. It is also assumed for the reduced volume state that if the band was removed from the eye, the eyeball would have the pressure $p_0 < p_t$ and, if returned to spherical shape, the radius r_0 satisfying (2.4) and $\mathcal{C}(r_0)[p] = p_t$. Thus, the mathematical problem to be solved for the postoperative state is to seek a radial function v and a reduced volume $V_0 = 4\pi r_0^3/3$ which satisfy $\mathcal{C}(r_0) = (v, p_t)$.

3. Solution procedures

Equations (2.26) and (2.25) are solved by the following approximate Newton iteration:

$$\begin{bmatrix} A(v) & K(v) \\ K^*(v) & 0 \end{bmatrix} \begin{bmatrix} u \\ \lambda \end{bmatrix} = \begin{bmatrix} B(v, p) \\ E(v) \end{bmatrix}, \tag{3.1}$$

$$v = v + \alpha u, \quad p = p + \alpha\lambda, \quad \alpha \in (0, 1], \tag{3.2}$$

in which only the derivatives of the left sides of (2.26) and (2.25) are used in the Jacobian of (3.1). The updates u and λ on v and p continue until (3.1) is solved by $u \approx 0$ and $\lambda \approx 0$. As explained in detail below, B and E represent the equation residuals for (2.26) and (2.25), respectively. Existence of a weak solution (u, λ) to (3.1) can be established as shown in Appendix A.

Equation (2.26) is represented in the first component of (3.1), which includes the following operators:

$$A(v)u = -\left\{ \frac{T(v)v\sin\phi}{\sqrt{v^2 + v_\phi^2}} u_\phi \right\}_\phi + \frac{T(v)v\sin\phi}{\sqrt{v^2 + v_\phi^2}} u, \tag{3.3}$$

$$K(v)\lambda = -\lambda v^2 \sin\phi \tag{3.4}$$

and for $v \in \mathcal{D}(A) = \{u \in \mathcal{H}^2([0, \pi]) : u_\phi = 0, \phi = 0, \pi\}$,

$$B(v, p) = -A(v)v - T(v)\sin\phi\sqrt{v^2 + v_\phi^2} + \left[f(v\sin\phi, v\cos\phi)\frac{(v\cos\phi)_\phi}{\sqrt{v^2 + v_\phi^2}} + p \right] v^2 \sin\phi. \tag{3.5}$$

Equation (2.25) is represented in the second component of (3.1), which includes the operators:

$$K^*(v)u = -\int_0^\pi uv^2 \sin\phi \, \mathrm{d}\phi \tag{3.6}$$

and

$$E(v) = \int_0^\pi v^3 \sin\phi \, \mathrm{d}\phi - 2r_1^3. \tag{3.7}$$

Thus, for the intraoperative state, the desired v and p are found by the iteration in (3.1) using the starting values $v = r_1$ and $p = p_1$. Given this procedure, the equation $\mathcal{C}(r_0) = (v, p_t)$ is solved for the postoperative state as follows:

1. Set $p_b = p_t$ and compute the associated band-free radius r_b from (2.4). Then, determine $\mathcal{C}(r_b)$ by iteration of (3.1) and (3.2) using starting conditions $v = r_b$ and $p = p_b$.
2. Set $r_a = \hat{R}$, where $\hat{R}$ is the given rest radius of the cerclage, and compute the associated band-free pressure p_a from (2.4). Since the band exerts no force at this radius, $\mathcal{C}(r_a) = (v = r_a, p = p_a)$ holds.
3. Since $\mathcal{C}(r_a)[p] < p_t < \mathcal{C}(r_b)[p]$ holds, use the interval $[r_a, r_b]$ to start a bisection method to solve $\mathcal{C}(r_0)[p] = p_t$ for r_0 by iteration of (3.1) and (3.2). The associated pressure p_0 is determined from (2.4).
4. The desired radial function is given by $\mathcal{C}(r_0)[v]$.

4. Numerical formulation

Equation (3.1) is discretized by finite differences as follows. Let the interval $[0, \pi]$ be divided into N cells with cell centres $\phi_i = \left(i - \frac{1}{2}\right)h$, $h = \pi/N$, $1 \leqslant i \leqslant N$, and cell boundaries $\phi_{i+\frac{1}{2}} = ih$, $0 \leqslant i \leqslant N$. Also, let $\bar{v}$ and $\bar{u}$ denote the vectors of v- and u-values, respectively, at the cell centres. Then, $A(v)u$ is approximated at the cell centre ϕ_i by

$$h^2[A_h(\bar{v})\bar{u}]_i = a_{i+\frac{1}{2}}(\bar{v}, p)[u_{i+1} - u_i] - a_{i-\frac{1}{2}}(\bar{v}, p)[u_i - u_{i-1}] + h^2 a_i u_i, \quad 1 \leqslant i \leqslant N, \tag{4.1}$$

where

$$a_i = \frac{T(\bar{v})v_i \sin\phi_i}{\sqrt{v_i^2 + Dv_i^2}}, \quad 1 \leqslant i \leqslant N, \quad a_{i+\frac{1}{2}} = \frac{a_{i+1} + a_i}{2}, \quad 0 < i < N, \tag{4.2}$$

and

$$Dv_i = \frac{v_{i+1} - v_{i-1}}{2h}, \quad \text{where } v_0 = 2v_1 - v_2, \quad v_{N+1} = 2v_N - v_{N-1}. \tag{4.3}$$

Note that $\sin\phi$ in a_i is never evaluated on the boundary and thus $a_i > 0$. On the other hand, because of boundary conditions, $a_{\frac{1}{2}} = 0 = a_{N+\frac{1}{2}}$ holds. Next, $K(v)\lambda$ is approximated at the cell centre ϕ_i by

$$[K_h(\bar{v})\lambda]_i = [K_h(\bar{v})]_i \lambda = -\lambda v_i^2 \sin\phi_i, \quad 1 \leqslant i \leqslant N, \tag{4.4}$$

and $K^*(v)u$ by

$$K_h^*(\bar{v})\bar{u} = -h\sum_{i=1}^{N} u_i v_i^2 \sin\phi_i = hK_h^\top(\bar{v})\bar{u}. \tag{4.5}$$

For the right side of (3.1), $B(v, p)$ is approximated at the cell centre ϕ_i by

$$[B_h(\bar{v}, p)]_i = -[A_h(\bar{v})\bar{v}]_i - T(\bar{v}) \sin\phi_i \sqrt{v_i^2 + Dv_i^2} + \left[f(v_i \sin\phi_i, v_i \cos\phi_i) \frac{Dv_i \cos\phi_i - v_i \sin\phi_i}{\sqrt{v_i^2 + Dv_i^2}} \right] v_i^2 \sin\phi_i \tag{4.6}$$

and $E(v)$ by

$$E_h(\bar{v}) = h \sum_{i=1}^{N} v_i^3 \sin\phi_i - 2r_1^3. \tag{4.7}$$

So (3.1) is discretized with a symmetric coefficient matrix according to

$$\begin{bmatrix} A_h(\bar{v}) & K_h(\bar{v}) \\ K_h^\top(\bar{v}) & 0 \end{bmatrix} \begin{bmatrix} \bar{u} \\ \lambda \end{bmatrix} = \begin{bmatrix} B_h(\bar{v}, p) \\ h^{-1} E_h(\bar{v}) \end{bmatrix}. \tag{4.8}$$

The update

$$\bar{v} = \bar{v} + \alpha\bar{u}, \quad p = p + \alpha\lambda \tag{4.9}$$

is performed first with $\alpha = 1$, and in case of divergence, the iteration is restarted and α is reduced until convergence is achieved.

5. Model validation

In order to test the predictive capability of our model, we first determine the material properties of the eyeball and the band by means that are independent from our simulations. The results of this parameter determination are shown in Table 1. Then, we describe an experiment with an enucleated eye which was deformed by the application of a cerclage. The results of this experiment are summarized in Table 2. Finally, these experimental results are simulated with our model, using the parameters shown in Table 3, and measured values are compared with computed values in Table 2. The simulation results are specified in greater detail in Table 4 and they are also shown graphically in Fig. 3.

5.1 *Determination of material properties*

The cerclage used was rectangular with width $\omega_b = 2$ mm and thickness $\delta_b = 0.75$ mm. By measuring the ratio of stress to strain in straight-line bands of this type of cerclage, the Young's modulus was determined to be $E_b = 24453$ mmHg. These measurements are a courtesy of the Austrian company 'Messphysik Materials Testing GmbH'. The rest radius of the cerclage, $\hat{R} = 10.35$, was determined by measuring the length of the unstretched restraightened band after the experiment as described in Section 5.2.

Aside from the cornea and the lens as well as all other inhomogeneities of the eyeball, the outer layers of the eyeball are the sclera and the choroid. Data for the elastic properties of these two layers of the surface of enucleated human eyeballs are reported in Friberg & Lace (1988). The measurements were conducted on rectangular strips that were cut out of the two layers at several locations and orientations.

TABLE 1 *Measured eyeball and cerclage parameters*

Measured eyeball parameters		Measured cerclage parameters	
Young's modulus E_{m}	16232 mmHg	Young's modulus E_{b}	24453 mmHg
Thickness δ_{m}	1 mm	Thickness δ_{b}	0.75 mm
Ocular rigidity σ	1/80	Width ω_{b}	2 mm
		Rest radius $\hat{R}$	10.35 mm

TABLE 2 *Measured and computed preoperative, intraoperative and postoperative states*

		Measured	Computed
Preoperative	p_1 (mmHg)	23.00	
	r_1 (mm)	12.25	
Intraoperative	$\mathcal{C}(r_1)[p]$ (mmHg)	76.00	59.82
	$\min \mathcal{C}(r_1)[v]$ (mm)	11.94	10.89
Postoperative	$\mathcal{C}(r_0)[p]$ (mmHg)	20.00	20.00
	$\min \mathcal{C}(r_0)[v]$ (mm)	11.22	10.44

TABLE 3 *Input parameters for the simulation shown in Fig.* 3

r_1	12.25 mm	E_{b}	24453 mmHg	E_{m}	16232 mmHg	σ	1/80
p_1	23 mmHg	δ_{b}	0.75 mm	δ_{m}	1 mm	α	0.5
p_{t}	20 mmHg	$-z_1, z_2$	1 mm	$\hat{R}$	10.35 mm	N	101

TABLE 4 *Quantitative results for the simulation shown in Fig.* 3

Preoperative		Intraoperative	
p_1	23.00 mmHg	$\mathcal{C}(r_1)[p]$	59.82 mmHg
r_1	12.25 mm	$\min \mathcal{C}(r_1)[v]$	10.89 mm
		$\max \mathcal{C}(r_1)[v]$	13.69 mm
T_1	140.90 mm mmHg	$T(v)$	331.90 mm mmHg
Postoperative band free		Postoperative	
p_0	5×10^{-8} mmHg	$\mathcal{C}(r_0)[p]$	20.00 mmHg
r_0	11.34 mm	$\min \mathcal{C}(r_0)[v]$	10.44 mm
		$\max \mathcal{C}(r_0)[v]$	12.35 mm
T_0	3×10^{-7} mm mmHg	$T(v)$	104.9 mm mmHg

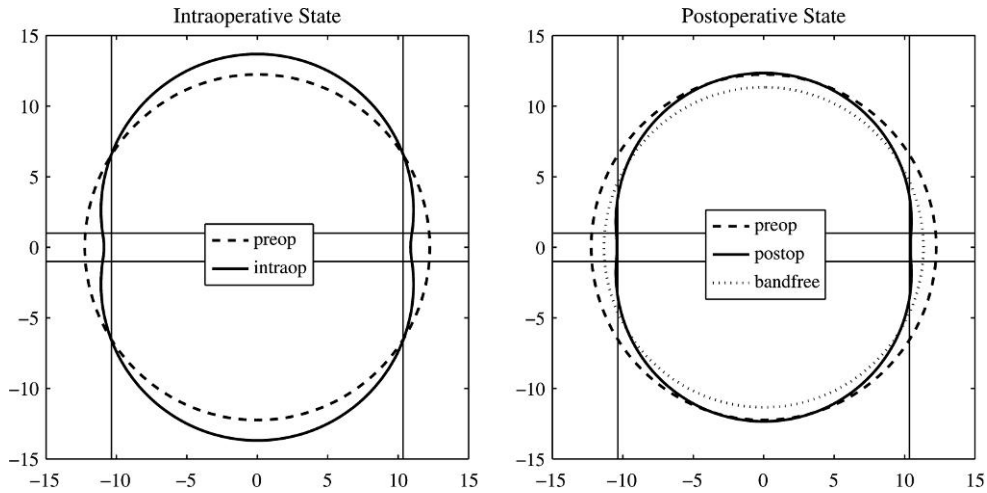

FIG. 3. Shown on the left are the (dashed) preoperative and (solid) intraoperative computed geometries of the eye. Shown on the right are the (dashed) preoperative, (solid) postoperative and the (dotted) postoperative band-free computed geometries of the eye. All curves are understood to be rotated about the central vertical axis consistent with the orientation of the eye shown in Fig. 2. The horizontal lines touch the eyeball geometries at opposite edges of the band. The vertical lines demonstrate the depth at which the band is at rest.

The average Young's moduli given in Friberg & Lace (1988) are $E_s = 2.3 \times 10^6$ Nm^{-2} for the sclera and $E_c = 6.0 \times 10^5$ Nm^{-2} for the choroid. Searching in Friberg & Lace (1988) for a uniform thickness of the two layers, we find 0.08 mm for the choroid and, somewhat indirectly on p. 434, 1 mm for the sclera. In Collins & van der Werff (1980, p. 2), it is stated that the thickness of the eye's covering, including the thinner cornea, varies between 0.3 and 1.3 mm. This leads us to the choice $\delta_m = 1$ mm for use in (2.5). The Young's modulus for the composite membrane is taken as the weighted average $E_m = (\delta_s E_s + \delta_c E_c)/(\delta_s + \delta_c)$ with $\delta_s = 0.92$ mm and $\delta_c = 0.08$ mm, so that $E_m = 16232$ mmHg.

In our experiments with an enucleated human eyeball, we first determined the coefficient of ocular rigidity σ. Stepwise injection of fluid into the eyeball and measurement of the corresponding intraocular pressure generated data points for the pressure/volume dependence. A fit to these data in the range $19 \leqslant p \leqslant 80$ mmHg leads to $\sigma = 1/80$ mm^{-3}. This value is small compared to the standard value $\sigma = 1/20$ given for instance in (2.66) of Collins & van der Werff (1980), but since our experiment was carried out on just this particular eyeball, we decided to use the smaller value for (2.4).

The measurements described above are listed in Table 1. Thus, with the exception of r_1, p_1 and $\hat{R}$, all model parameters have been set independently of the following experiment with an equatorial cerclage/eyeball configuration.

5.2 *Experiment with enucleated eyeball*

The experimental task was to determine the pre-, intra- and postoperative states as follows. First, the circumference of the undistorted eyeball was measured by twining a thin, inelastic thread around its equator. The corresponding radius is denoted by r_1 shown in the column of measured values in Table 2. Then, on top of the thread, the band was wound around the equator. The band is longer than the circumference of the equator and can be stretched by pulling its ends in opposite directions. Then, a closed stretched annular cerclage was made out of the middle third of the band by tying a special seam about

both arms of the band where they touch each other. This resulted in an annular stretched middle part of the band that has a fixed rest radius $\hat{R}$ which is smaller than r_1. The circumference of the slightly indented eyeball was determined by making a mark on the meanwhile tightened equatorial thread. The corresponding radius is shown next to $\min \mathcal{C}(r_1)[v]$ in the column of measured values in the intraoperative section of Table 2. Also, the two arms of the cerclage were marked at the closing seam. Then, the intraocular pressure was reduced by withdrawing aqueous humour through a needle that was inserted across the sclera beforehand. In living eyes, the reduction of interior pressure is a slow autoregulated process. In the experiment, the target was to go back to approximately nominal pressure within about a minute. Once this was achieved, the circumference of the new indentation was determined by making another mark on the re-tightened equatorial thread. The corresponding radius is shown next to $\min \mathcal{C}(r_0)[v]$ in the column of measured values in the postoperative section of Table 2. In all three stationary configurations, the intraocular pressure was measured, and these pressures are shown in Table 2 in the column of measured values next to p_1, $\mathcal{C}(r_1)[p]$ and $\mathcal{C}(r_0)[p]$ for the preoperative, intraoperative and postoperative states, respectively. Finally, the closing seam was opened, the cerclage removed and $\hat{R}$ determined by the distance of the two marks on the arms of the then unstretched restraightened band. Deviating from the typical case that $p_t = p_1$ holds, the postoperative pressure in the experiment ($p_t = 20$) is not the same as the preoperative pressure ($p_1 = 23$).

The thickness of the marks on the encircling band and on the thread turned out to be the main factor limiting the accuracy of the experiment. The thickness of the mark was about 1 mm, which is approximately 1.5% of the circumference of the eye. As the length of the encircling band and the thread was determined by measuring the distance between two marks, we suggest 3% of the measured length as an estimate for the accuracy limit. The eye pressure was measured using a commercially available device for intraocular measurements of eye pressure (Mod. Duesseldorf, Geuder, Heidelberg, Germany). As we did not have a sufficient number of experiments, no estimation of accuracy and error could be made and the measured intraocular pressure was considered to be accurate. The intraocular volume was reduced in steps of 0.05–0.1 ml. The scale on the syringe was in steps of 0.01 ml which therefore is the smallest measurable change of intraocular volume. As we increased the intraocular volume in steps of at least 0.05 ml, we expect the measurement error for change of intraocular volume to be less than 20%. Compared to the reported data, we had a relatively lower increase of intraocular pressure for a given volume, which needs further evaluation (Pallikaris *et al.*, 2005). As we did not evaluate the eyes used for concurrent pathology, the age of the donor and the postmortem time to experiment, i.e. those factors which have been discussed in literature as contributing to scleral rigidity, might have influenced our results (Silver & Geyer, 2000; Elsheikh *et al.*, 2008a).

5.3 *Simulation of experiment*

The measured values shown in Table 2 are compared with values computed from our model as follows. The material properties in Table 1 and the experimental values in Table 2 were used for the model input values shown in Table 3. In particular, for equatorial application of the cerclage, z_1, z_2 are set to $\mp\omega_b/2$. Although the nominal starting pressure is $p_1 = 23$ mmHg, the target pressure in the postoperative state is $p_t = 20$ mmHg, as explained in Section 5.2. Note also that the membrane was discretized with $N = 101$ cells and the relaxation level used was $\alpha = 0.5$. Using the parameters shown in Table 3, (2.25) and (2.26) are solved by the iterations (4.8) and (4.9), and the results are shown graphically in Fig. 3. Also, some additional results are summarized quantitatively in Table 4.

Shown on the left in Fig. 3 are the intraoperative and postoperative computed geometries of the eye. Shown on the right are the preoperative, postoperative and the postoperative band-free computed

geometries of the eye. All curves are understood to be rotated about the central vertical axis consistent with the orientation of the eye shown in Fig. 2. The horizontal lines are plotted at heights z_1 and z_2 and thus they touch the eyeball geometries at opposite edges of the band. The vertical lines demonstrate the depth at which the band is at rest. Note that the band may depart from a cylindrical shape as discussed in relation to (2.1), but the band assumes a roughly cylindrical shape when its width ω_b and the equatorial indentation $r_1 - \upsilon(\pi/2)$ are small in relation to the radius r_1. Shown in Fig. 4 is the history of the converging pressure plotted as a function of total iterations of (3.1) and (3.2) embedded in the bisection scheme of the algorithm shown in Section 3. Just before each jump in this graphic, the iteration (4.8) and (4.9) has just converged using the current estimate of postoperative band-free quantities (r_0, p_0). According to the algorithm, these estimations continue iteratively until $\mathcal{C}(r_0) = (\upsilon, p_t)$ holds. Specifically, in Fig. 4, the pressure begins and ends at 20 mmHg. So in the presence of the band load, the pressure returns to the target value p_t after the volume is reduced as demonstrated by the reduced radius $r_0 < r_1$ shown in Table 4. Note also in Table 4 that the postoperative band-free pressure and tension are essentially zero since the volume is so low that the pressure $\mathcal{C}(r_0)[p] = 20$ mmHg in the band-loaded state is essentially driven entirely by the band forces.

Recall that the band-free state r_0, p_0, T_0 is never attained in medical practice nor was it measured in the experiments with enucleated eyes; it is a hypothetical state determined by the algorithm such that the model predicts p_t when the band is applied to it. More precisely, r_0 is determined by bisection and p_0 and T_0 follow by (2.4) and (2.3).

The computed values in Table 2 do not differ greatly from the measured values shown in Table 2, but the predictions of the model do not precisely coincide with the measured data. More specifically, the predicted intraoperative pressure (59.82 mmHg) is about 21% smaller than the measured value (76.00 mmHg) and the predicted radius at the indentation (10.89 mm) is 9% smaller than the measured radius (11.94 mm). While the predicted postoperative pressure (20.00 mmHg) is required to match exactly the measured value (20.00 mmHg), the predicted radius at the indentation (10.43 mm) is 7% smaller than the measured radius (11.22 mm), which happens to match the band-free radius ($r_0 = 11.20$)

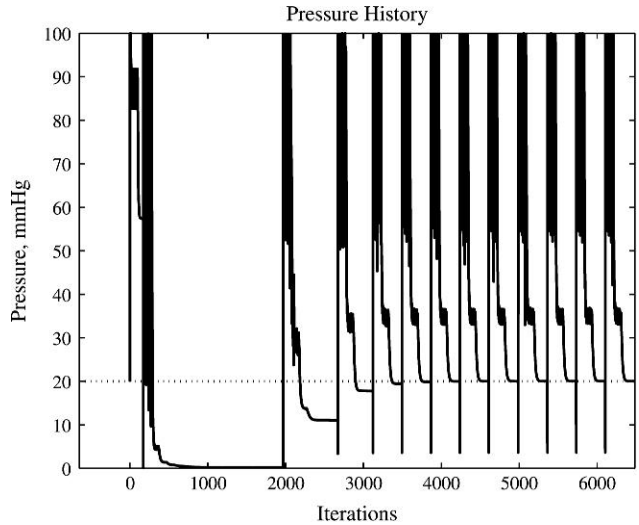

FIG. 4. For the calculation of the postoperative state shown on the right in Fig. 3, the history of the converging pressure is plotted as a function of total iterations of (3.1) and (3.2) embedded in the bisection scheme of the algorithm given in Section 3.

shown in Table 4 nearly exactly. Considering the simple methods of acquiring the data and the model parameters, we regard these deviations as tolerable. We want to stress that we did not fit the model parameters to the data in order to get minimal deviations. A more detailed validation of the model requires more systematic (still model independent) determination of the parameters and more elaborate experimental procedures. Here, we have reported a first test that confirms the applicability of our approach.

Our model differs from the real situation in that the sclera was modelled to be elastic with a Young's modulus that is assumed to remain constant. In reality, the sclera will not contract infinitely, below some minimum surface area. This non-linear behaviour has only little influence on intraocular pressure and the shape of the eye during and immediately after surgery, when the intraocular pressure is increased and the sclera is stretched, but it might be important for the final shape of the eye, when intraocular pressure has returned to normal and the sclera is contracting but stops when it has reached a particular minimum surface area. In fact, with the material properties listed in Table 1, our simulation predicts only a small change in the axial length of the eye between the preoperative and the postoperative states. This is in contrast to clinical results, which show elongation of the axial length in most cases (Malukiewicz-Winiewska & Stafiej, 1999). Nevertheless, this elongation can be obtained with our model when $E_{\mathrm{m}}\delta_{\mathrm{m}}$ in Table 1 is reduced moderately. Thus, the presented model gives a good estimate of intraocular pressure and shape for the intra- and immediate postoperative period with the reported material properties. Further improvements in modelling or in parameter determination need to be carried out to increase the accuracy of the final shape of the eye in the late postoperative period.

6. Conclusion

A simple model for the deformation of an eyeball caused by the application of an elastic band was derived. The model is a two-point boundary-value problem with a constraint for a non-linear second-order ordinary differential equation. The simplicity of the model stems from idealizing modelling approximations: the eyeball is treated as if it were a uniform spherical membrane filled with fluid. The two-point boundary-value problem is solved numerically by finite differences. Based on the model, an algorithm was presented that predicts the eye's indentation due to the application of the band. Such a prediction, that depends on the material properties of the band and its stretching, is of interest for planning the surgery and its effect. In particular, the algorithm was used to predict the maximal intraocular pressure immediately after surgery, as well as the final indentation of the eyeball, when the intraocular pressure is back to normal. By comparison with measurements on an enucleated human eye, it was found that the model's predictions are in reasonable agreement with the experimental data.

Funding

Keeling was supported by the Austrian Science Fund *Fonds zur Förderung der Wissenschaftlichen Forschung* (FWF) under grant SFB F032 with the webpage `http://math.uni-graz.at/mobis/`.

References

ADAMS, R. A. (1975) *Sobolev Spaces*. New York: Academic Press.

ADAMSON, A. (1997) *Physical Chemistry of Surfaces*, 6th edn. New York: Wiley.

ALASTRUÉ, V., CALVO, B., PEÑA, E. & DOBLARÉ, M. (2006) Biomechanical modeling of refractive corneal surgery. *J. Biomech. Eng.*, **128**, 150–160.

BLYTH, M. G. & POZRIKIDIS, C. (2004) Solution space of axisymmetric capsules enclosed by elastic membranes. *Eur. J. Mech. A*, **23**, 877–892.

BRYANT, M. R. & MCDONNELL, P. J. (1996) Constitutive laws for biomechanical modeling of refractive surgery. *J. Biomech. Eng.*, **118**, 473–481.

CIARLET, P. G. (1978) *The Finite Element Method for Elliptic Problems*. Amsterdam: North-Holland.

COLLINS, R. & VAN DER WERFF, T. J. (1980) *Mathematical Models of the Dynamics of the Human Eye*. Lecture Notes in Biomathematics. Berlin: Springer.

ELSHEIKH, A., ALHASSO, D. & RAMA, P. (2008a) Biomechanical properties of human and porcine corneas. *Exp. Eye Res.*, **86**, 783–790.

ELSHEIKH, A., BROWN, M., ALHASSO, D., RAMA, P., CAMPANELLI, M. & GARWAY-HEATH, D. (2008b) Experimental assessment of corneal anisotropy. *J. Refract. Surg.*, **24**, 178–187.

FRIBERG, T. R. & LACE, J. W. (1988) A comparison of the elastic properties of human choroid and sclera. *Exp. Eye Res.*, **47**, 429–436.

GONIN, J. (1920) Pathogenie et anatomie pathalogique des decollements retiens. *Bull. Mem. Soc. Fr. Ophthalmol.*, **33**, 1–123.

HEIMANN, H., BARTZ-SCHMIDT, K. U., BORNFELD, N., WEISS, C., HILGERS, R. D. & FOERSTER, M. H. (2007) Scleral buckling versus primary vitrectomy in rhegmatogenous retinal detachment: a prospective randomized multicenter clinical study. *Ophthalmology*, **114**, 2142–2154.

HOELTZEL, D. A., ALTMAN, P., BUZARD, K. & CHOE, K. (1992) Strip extensiometry for comparison of the mechanical response of bovine, rabbit, and human corneas. *J. Biomech. Eng.*, **114**, 202–215.

MALUKIEWICZ-WINIEWSKA, G. & STAFIEJ, J. (1999) Changes in axial length after retinal detachment surgery. *Eur. J. Ophthalmol.*, **9**, 115–119.

PALLIKARIS, I. G., KYMIONIS, G. D., GINIS, H. S., KOUNIS, G. A. & TSILIMBARIS, M. K. (2005) Ocular rigidity in living human eyes. *Invest. Ophthalmol. Vis. Sci.*, **46**, 409–414.

PANDOLFI, A. & MANGANIELLO, F. (2006) A model for the human cornea: constitutive formulation and numerical analysis. *Biomech. Model. Mechanobiol.*, **5**, 237–246.

PELLICER, J., MANZANARES, J. A. & MAFÉ, S. (1995) The physical description of elementary surface phenomena: thermodynamics versus mechanics. *Am. J. Phys.*, **63**, 542–547.

PINSKY, P. M., VAN DER HEIDE, D. & CHERNYAK, D. (2005) Computational modeling of mechanical anisotropy in the cornea and sclera. *J. Cataract Refract. Surg.*, **31**, 136–145.

PRESTON, S. P., JENSEN, O. E. & RICHARDSON, G. (2008) Buckling of an axisymmetric vesicle under compression: the effects of resistance to shear. *Q. J. Mech. Appl. Math.*, **61**, 1–24.

PURSLOW, P. P. & KARWATOWSKI, W. S. S. (1996) Ocular elasticity. *Ophthalmology*, **103**, 1686–1692.

SCHEPENS, C. L., OKAMURA, L. D. & BOCKHURST, L. J. (1957) The scleral buckling procedures. I. Surgical techniques and management. *AMA Arch. Ophthalmol.*, **58**, 797–811.

SCHMITZ-VALCKENBERG, P. & MEYER-SCHWICKERATH, G. (1975) Kontrollierter Zug bei der Cerclage-Operation. *Albrecht Von Graefes Arch. Klin. Exp. Ophthalmol.*, **197**, 89–99.

SEO, G., PARK, C., ADLAND, Z. & LEE, J. (2003) Ocular mechanics—quantitative modeling and analyses of the eyeball. *Report No. T3EyeFinalRep566S03*. Tucson, AZ: Department of Aerospace and Mechanical Engineering, University of Arizona.

SILVER, D. M. & GEYER, O. (2000) Pressure-volume relation for the living human eye. *Curr. Eye Res.*, **20**, 115–120.

Appendix A. Existence of a solution (u, λ)

Existence of a weak solution (u, λ) to (3.1) is established as follows. Define the (v, p)-dependent bilinear form

$$\mathcal{B}(u, \bar{u}; v, p) = \int_0^{\pi} \left\{ \frac{T(v)v}{\sqrt{v^2 + v_\phi^2}} \right\} [u_\phi \bar{u}_\phi + u\bar{u}] \sin\phi \, \mathrm{d}\phi \tag{A.1}$$

which satisfies

$$\mathcal{B}(u,\bar{u};\upsilon,p)=(A(\upsilon)u,\bar{u})_{L^2([0,\pi])},\quad \forall u,\bar{u}\in\mathcal{D}(A). \tag{A.2}$$

For this, it is assumed that $\upsilon\in W^{1,\infty}([0,\pi])$ satisfies

$$\upsilon\geqslant\varepsilon>0 \tag{A.3}$$

and

$$\|\upsilon\|_{W^{1,\infty}([0,\pi])}\leqslant\beta. \tag{A.4}$$

To obtain the positivity of the coefficient in (A.1), it is assumed that the following holds:

$$E_{\mathrm{m}}\delta_{\mathrm{m}}\leqslant T_0\equiv\tfrac{1}{2}r_0p_1\exp\left[\frac{4\pi\sigma}{3}(r_0^3-r_1^3)\right], \tag{A.5}$$

where $V_0=4\pi r_0^3/3$ is the constant volume to which υ is constrained,

$$\int_0^\pi \upsilon^3\sin\phi\,\mathrm{d}\phi=2r_0^3 \tag{A.6}$$

and thus $r_0(\upsilon)$ in (2.6) is the constant r_0 in (A.6). Then, it follows from (2.7) that $T_0(\upsilon)=T_0$ in (A.5). Since the surface area of a given volume is always minimized with a spherical geometry, it follows that $S(\upsilon)\geqslant S(r_0(\upsilon))=S(r_0)$. Thus, $T(\upsilon)$ in (2.5) satisfies

$$T(\upsilon)=[T_0-E_{\mathrm{m}}\delta_{\mathrm{m}}]+E_{\mathrm{m}}\delta_{\mathrm{m}}\frac{S(\upsilon)}{S(r_0(\upsilon))}\geqslant E_{\mathrm{m}}\delta_{\mathrm{m}} \tag{A.7}$$

when (A.5) holds. Combining the estimates above gives the following lower bound on the coefficient in (A.1):

$$\frac{T(\upsilon)\upsilon}{\sqrt{\upsilon^2+\upsilon_\phi^2}}\geqslant\frac{E_{\mathrm{m}}\delta_{\mathrm{m}}\upsilon}{\sqrt{\upsilon^2+\upsilon_\phi^2}}\geqslant\frac{E_{\mathrm{m}}\delta_{\mathrm{m}}\varepsilon}{\sqrt{2}\beta}\equiv c_1. \tag{A.8}$$

From (2.8), (A.3) and (A.4), $S(\upsilon)$ satisfies

$$S(\upsilon)=2\pi\int_0^\pi \upsilon\sin\phi\sqrt{\upsilon^2+\upsilon_\phi^2}\,\mathrm{d}\phi\leqslant 4\pi\sqrt{2}\beta^2, \tag{A.9}$$

while $S(r_0)=4\pi r_0^2$ holds, and thus, the following upper bound on the coefficient in (A.1) is obtained:

$$\frac{T(\upsilon)\upsilon}{\sqrt{\upsilon^2+\upsilon_\phi^2}}=\frac{\upsilon}{\sqrt{\upsilon^2+\upsilon_\phi^2}}\left\{T_0+E_{\mathrm{m}}\delta_{\mathrm{m}}\left[\frac{S(\upsilon)}{S(r_0)}-1\right]\right\}\leqslant T_0+E_{\mathrm{m}}\delta_{\mathrm{m}}\left[\sqrt{2}\frac{\beta^2}{r_0^2}-1\right]\equiv c_2. \tag{A.10}$$

Thus, it follows that B is bounded and coercive on $\mathcal{H}^1([0,\pi])$:

$$c_1\|u\|^2_{\mathcal{H}^1([0,\pi])}\leqslant|\mathcal{B}(u,u;\upsilon,p)|,\quad |\mathcal{B}(u,\bar{u};\upsilon,p)|\leqslant c_2\|u\|_{\mathcal{H}^1([0,\pi])}\|\bar{u}\|_{\mathcal{H}^1([0,\pi])}. \tag{A.11}$$

By the Lax–Milgram Theorem (Ciarlet, 1978), there is a linear operator $\hat{A}(v, p)$ which is bounded on $\mathcal{H}^1([0, \pi])$ and satisfies

$$\mathcal{B}(u, \bar{u}; v, p) = (\hat{A}(v, p)u, \bar{u})_{\mathcal{H}^1([0,\pi])}, \quad \forall u, \bar{u} \in \mathcal{H}^1([0, \pi]). \tag{A.12}$$

For a given v satisfying (A.4), define the operator $\hat{K}(v)$: $\boldsymbol{R} \to \mathcal{H}^0([0, \pi])$ by

$$\hat{K}(v)\lambda = -\lambda v^2. \tag{A.13}$$

Then, by (3.4) and (A.13), $\hat{K}$ satisfies

$$(\hat{K}(v)\lambda, u)_{\mathcal{H}^0([0,\pi])} = (K(v)\lambda, u)_{L^2([0,\pi])}, \quad \forall u \in \mathcal{H}^0([0, \pi]). \tag{A.14}$$

For a given v satisfying (A.4), define the function

$$\hat{B}(v, p) = -\hat{A}(v, p)v - T(v)\sqrt{v^2 + v_\phi^2} + [f(v \sin\phi, v \cos\phi)(v \cos\phi)_\phi / \sqrt{v^2 + v_\phi^2} + p]v^2. \tag{A.15}$$

Then, using (3.5), (A.2) and (A.12), $\hat{B}$ satisfies the following for $v \in \mathcal{D}(A)$:

$$(\hat{B}(v, p), u)_{\mathcal{H}^0([0,\pi])} = (B(v, p), u)_{L^2([0,\pi])}, \quad \forall u \in \mathcal{H}^0([0, \pi]). \tag{A.16}$$

According to (3.6), the adjoint of $\hat{K}(v)$ is given by

$$\hat{K}^*(v)u = K^*(v)u. \tag{A.17}$$

To complete the transformation of (3.1), define

$$\hat{E}(v) = E(v) \tag{A.18}$$

to obtain that

$$\begin{bmatrix} \hat{A}(v, p) & \hat{K}(v) \\ \hat{K}^*(v) & 0 \end{bmatrix} \begin{bmatrix} u \\ \lambda \end{bmatrix} = \begin{bmatrix} \hat{B}(v, p) \\ \hat{E}(v) \end{bmatrix}. \tag{A.19}$$

Solving for u and λ leads to the relations

$$\begin{aligned} [\hat{K}^*(v)\hat{A}^{-1}(v, p)\hat{K}(v)]\lambda &= \hat{K}^*(v)\hat{A}^{-1}(v, p)\hat{B}(v, p) - \hat{E}(v), \\ u &= \hat{A}^{-1}(v, p)[\hat{B}(v, p) - \hat{K}(v)\lambda]. \end{aligned} \tag{A.20}$$

Thus, u is given in terms of λ, which is determined by the first equation provided it can be shown that the constant $[\hat{K}^*(v)\hat{A}^{-1}(v, p)\hat{K}(v)]1$ does not vanish. For this, the constant is written as

$$[\hat{K}^*(v)\hat{A}^{-1}(v, p)\hat{K}(v)]1 = \hat{K}^*(v)w, \tag{A.21}$$

where w is the solution to

$$\hat{A}(v, p)w = \hat{K}(v)1 = -v^2. \tag{A.22}$$

Then, the desired result is obtained once it is shown that $w \in C^0(0,\pi)$ and $0 \geqslant w \not\equiv 0$ hold, since for v satisfying (A.3), it follows from (3.6) that the constant in (A.21) satisfies $\hat{K}^*(v)w < 0$. Since w satisfies (A.22), which is given explicitly in (A.12), it follows that

$$\int_0^\pi \left\{ \frac{T(v)v}{\sqrt{v^2+v_\phi^2}} \right\} [w_\phi \bar{u}_\phi + w\bar{u}] \sin\phi \, \mathrm{d}\phi = -\int_0^\pi v^2 \bar{u} \sin\phi \, \mathrm{d}\phi, \quad \forall\, \bar{u} \in \mathcal{H}^1([0,\pi]). \tag{A.23}$$

Because of the estimate

$$\begin{aligned} \sin\varepsilon \int_\varepsilon^{\pi-\varepsilon} [w^2 + w_\phi^2] \mathrm{d}\phi &\leqslant \int_\varepsilon^{\pi-\varepsilon} [w^2 + w_\phi^2] \sin\phi \, \mathrm{d}\phi \\ &\leqslant \int_\varepsilon^{\pi-\varepsilon} [w^2 + w_\phi^2] \mathrm{d}\phi, \quad \forall\, \varepsilon > 0, \end{aligned} \tag{A.24}$$

it follows for $w \in \mathcal{H}^1([0,\pi])$ that $w \in H^1([\epsilon, \pi-\epsilon])$ for every $\epsilon > 0$. It follows from the Sobolev embedding theorem (Adams, 1975) that $w \in C^0(0,\pi)$. Thus, for the sake of contradiction, suppose that

$$w(\phi) > 0, \quad \phi \in (a,b) \subset (0,\pi). \tag{A.25}$$

Then, let $\psi \in W^{1,\infty}([0,\pi])$ be the non-negative function supported precisely on (a,b) and satisfying $\psi = \frac{1}{2}|\psi_\phi|$. Finally, set $\bar{u} = \psi w$ in (A.23) to obtain that

$$\begin{aligned} -\int_a^b v^2 w\psi \sin\phi \, \mathrm{d}\phi &= \int_a^b \left\{ \frac{T(v)v}{\sqrt{v^2+v_\phi^2}} \right\} [(w_\phi^2 + w^2)\psi + w_\phi w \psi_\phi] \sin\phi \, \mathrm{d}\phi \\ &\geqslant \int_a^b \left\{ \frac{T(v)v}{\sqrt{v^2+v_\phi^2}} \right\} \left[(w_\phi^2 + w^2)\psi - \tfrac{1}{2}(w_\phi^2 + w^2)|\psi_\phi| \right] \sin\phi \, \mathrm{d}\phi \\ &= 0. \end{aligned} \tag{A.26}$$

Then, it follows with (A.3) and (A.25) that the left side of (A.26) is strictly negative. The contradiction of (A.26) implies that $w \leqslant 0$ holds on $[0,\pi]$. Because of (A.3), it follows from (A.22), (A.12) and (A.11) that $w \not\equiv 0$ holds. From (A.17), (A.3) and (3.6), it follows that $\hat{K}^*(v)w$ in (A.21) satisfies $\hat{K}^*(v)w = K^*(v)w \neq 0$. Thus, λ and u are well defined by (A.20).